

## Study of residual stresses during electron beam welding of alloyed steels using neutron diffraction

P. Petrov<sup>1</sup>, D. Kaisheva<sup>1,\*</sup>, G. Bokuchava<sup>2</sup>, I. Papushkin<sup>2</sup>

<sup>1</sup>*Institute of Electronics of the Bulgarian Academy of Sciences, 72 Tzarigradsko Chaussee, 1784 Sofia, Bulgaria*

<sup>2</sup>*Frank Laboratory of Neutron Physics, Joint Institute for Nuclear Research, 6 Joliot-Curie Str., 141980 Dubna, Russia*

Received: July 14, 2017; Revised: October 28, 2017

In this work the results from studies of residual stresses of plates of alloyed steel welded using electron beam welding technology (EBW) are presented. The chemical composition of the first and the second welded plate is respectively (wt %): 0.11% C; 0.27% Si; 1.35% Cr; 0.6% Mn; 3.25% Ni and 0.08% C; 1% Si; 2% Mn; 0.045% P; 0.03% S; 8-10.5%Ni; 18-20% Cr. EBW was carried out on the ESW300 / 15-60 welding units manufactured by Leybold-Heraeus at the Institute of Electronics – BAS. The technological parameters of the EBW process were the following: accelerating voltage  $U = 60$  kV; beam current  $I = 50$  mA, welding speed  $V = 0.5$  cm/s; 1 cm/s; 2 cm/s, focusing lens-specimen distance  $D_0 = 38$  cm. The measurement of residual stresses was carried out at the Laboratory of Neutron Physics of the Joint Institute for Nuclear Research - Dubna, Russia. The flow of neutrons obtained by pulsed fast reactor IBR-2 was used. The diffraction spectra were obtained on a Fourier stress diffractometer FSD, located on the channel №11a of the reactor. The temperature fields in EBW of both of the alloyed steels were calculated.

**Keywords:** Residual stresses, Neutron diffraction, Alloyed steels, Temperature fields

### INTRODUCTION

As a result of the local heating during welding and the non-uniform temperature distribution residual stresses and distortions occur in the welded joint. They can significantly reduce the quality and reliability of the welded components [1]. Fig. 1 presents schematically the changes in the temperature - stress diagrams for the different cross-sections of a plate when the weld is not instantly realized over the entire length [2, 3]. In the cross-section A-A before the heat source, the temperature is constant and is assumed to be zero, and there are no stresses. The cross-section B-B, just after the welding source, is the most heated one. The temperature in the weld and the heat-affected zone (HAZ) rapidly increases, inducing compressive stresses there, since the cold regions of the base metal prevent their free expansion. These stresses are relatively weak, because the metal heated to a very high temperature has a low yield stress. In accordance with the counter-balance conditions, these weak compressive stresses cause weak tensile stresses in the adjacent cold regions. Since the yield stress in the heated zone is low, compressive plastic strains are induced. Over the cross-section C-C the joint is mainly in a cooling phase. The maximal temperatures and the temperature gradients decrease. The compressive stresses turn into tensile, since the heated metal has the tendency to shrink, which is prevented by the adjacent zones. When the

tensile stresses reach the yield stress for the respective temperature, tensile plastic strains form, which partly compensate the compressive plastic strains accumulated during heating. After complete cooling of the last cross-section considered, D-D, the longitudinal residual tensile stresses remain at the yield stress, and the adjacent zones of the welded joint remain compressed. The total residual longitudinal strain corresponds to a decrease in the plate length. The stress diagrams obtained are typical for metals without phase transformation during the welding process [3].

In accordance with the above, the main reason for the occurrence of the welding stress is the uniform distribution of the temperature field in the cross section of the welded samples. In the practice for the investigation of the residual stresses and distortions during welding there are two approaches: experimental and numerical modeling.

The mathematical methods allow obtaining relatively quick results of the final state and of the thermo-mechanical history. However, the precision of the results strongly depends on the exactness of the mathematical modeling of the welding process. Because the welding process and the resulting mechanical mechanism are very complex, many physical phenomena have to be taken into account. The accuracy of the numerical simulation of welding depends on the precision of the mathematical modeling of the heat input and the thermo-mechanical behaviour [2, 3].

\* To whom all correspondence should be sent.

E-mail: darinakaisheva@abv.bg

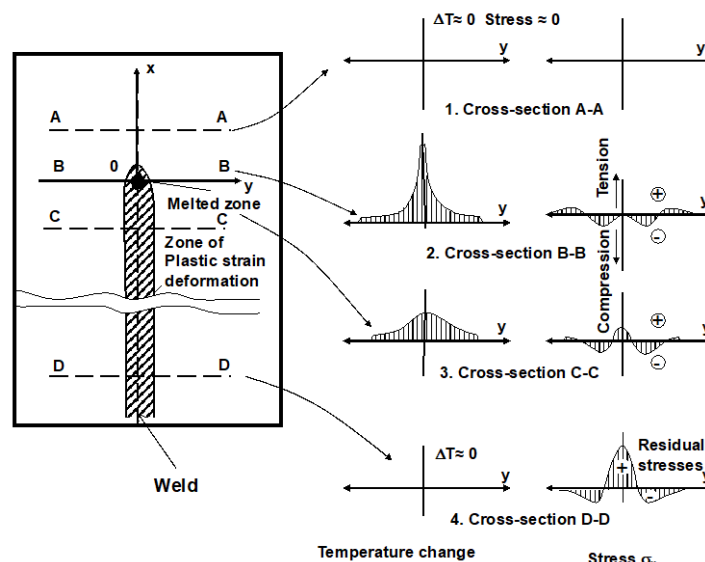


**Fig. 1.** Schematic presentation of the changes in the distribution of the temperature and longitudinal stress during welding of the plate [2]

The experimental investigations are very expensive and costly in terms of time (time-consuming). The results display only the final state without monitoring of the material behaviour during the process. The experimental methods can require a local or complete destruction of the objects. Residual stresses can be measured by various destructive or non-destructive methods [4].

The neutron diffraction method [5, 6] has a number of advantages over other methods, such as: preservation of the integrity of the studied sample, as the method is non-destructive; large depth of penetration of neutrons and a possibility for measuring to a large depth - up to 6 cm for steel and up to 10 cm for aluminum; possibility to measure macrostresses and microstresses; possibility to study samples of a random shape; high resolution of the gauge volume in the sample - up to 1 mm in any direction; possibility to determine the deformation in different directions of the crystal and to study the pattern of anisotropy of the deformation in different planes [hkl]; possibility to study the distribution of stress for each phase of multiphase material separately; high resolution of the diffractometer and possibility to measure relative deformation close to  $10^{-3}$ - $10^{-4}$ ; high accuracy for stress determination - 20-40 MPa (10 MPa - for aluminum, 30 MPa - for steel, 15 MPa - for titanium); possibility to estimate

microstresses, density of the dislocations and spot defects in the material *via* analyzing the shape and width of the diffraction maxima [7, 8].

In this work residual stresses of alloyed steels during electron beam welding were measured by the neutron diffraction method. Results from theoretical calculation of the temperature fields during electron beam welding are presented too.

#### EXPERIMENT AND MODELING

The welded specimens of two kinds of steel (chrome-nickel steel X5CrNi18-10 and constructive alloyed steel 12XH3A) were examined. Electron beam welding (EBW) was carried out on the ESW300/15-60 welding units manufactured by Leybold-Heraeus at the Institute of Electronics "Acad. E. Djakov", Bulgarian Academy of Sciences, Sofia, Bulgaria.

The technological parameters of the EBW process were the following: accelerating voltage  $U = 60$  kV; beam current  $I = 50$  mA; welding speed  $V$  from 0.5 to 2 cm/s; focusing lens - specimen distance  $D_0 = 38$  cm.

Table 1 contains data on the chemical composition of the studied samples. Table 2 contains data on the thermophysical parameters of the studied materials, which were used for calculation of temperature fields.

**Table 1.** Chemical composition.

	Element	C	Si	Cr	Mn	Ni	P	S
12XH3A	w, %	0.11	0.27	1.35	0.6	3.25		
X5CrNi18-10	w, %	0.08	1	18-20	2	8-10.5	0.045	0.03

**Table 2.** Thermophysical parameters.

	$\lambda,$ W/(mm.K)	$\rho,$ kg/m <sup>3</sup>	$C,$ J/(kg.K)	$a,$ mm <sup>2</sup> /s
12XH3A	0.0270	7680	540	6,510
X5CrNi18-10	0.0215	7920	550	4.936

### Experimental Residual Stresses Distributions

Residual stresses in welded specimens were measured at the Frank Laboratory of Neutron Physics, Joint Institute for Nuclear Research, Dubna, Russia on a Fourier stress diffractometer (FSD) [7, 8] on a fast pulsed IBR-2 reactor. FSD diffractometer is dedicated for residual stress studies in bulk industrial components and new advanced materials. A fast Fourier chopper for the primary neutron beam intensity modulation and the RTOF method for data acquisition make it possible to obtain high resolution neutron diffraction spectra  $\Delta d/d \approx 4 \times 10^{-3}$ .

Internal stresses existing in a material, causing respective lattice strains, result in shifts of Bragg peaks in the diffraction spectrum. This yields direct information on changes in interplanar spacing in a gauge volume, which can be transformed into data on residual stresses, using known elastic constants of a material:

$$\frac{(d_{exp} - d_0)}{d_0} = \frac{\Delta a}{a_0} \approx \frac{\sigma}{E} \quad (1)$$

where  $d_{exp}$  is the measured interplanar spacing,  $d_0$  is the same interplanar spacing in the sample without internal stresses,  $\Delta a/a_0$  is the strain as the relative change in the unit cell parameter of a material,  $E$  is the Young's modulus of a material, and  $\sigma$  is the stress.

The principle of determining the crystal lattice strain is based on the Bragg's law, showing the condition of diffraction maximum:

$$n\lambda = 2d_{hkl} \sin\theta \quad (2)$$

where  $\lambda$  is the neutron wavelength,  $d_{hkl}$  is the interplanar spacing, and  $\theta$  is the Bragg angle or the angle of incidence and scattered rays,  $n$  is an integer.

When using TOF diffraction method at a pulsed neutron source, the strain is determined by the relative change in the neutron time of flight  $\Delta t/t$ . Depending on the neutron wavelength, the peak position on the time scale is defined by the condition:

$$t = \frac{L}{v} = \frac{\lambda mL}{h} = \frac{2mLd_{hkl} \sin\theta}{h} \quad (3)$$

where  $L$  is the total flight distance from a neutron source to the detector,  $v$  is the neutron velocity,  $m$  is the neutron mass,  $h$  is Planck's constant.

Hence, in case of TOF neutron diffraction the lattice strain is determined as:

$$\varepsilon_{hkl} = \frac{d_{hkl} - d_{hkl}^0}{d_{hkl}^0} = \frac{\Delta t}{t} \quad (4)$$

where  $d_{hkl}$  and  $d_{hkl}^0$  are the interplanar spacings for strained and unstrained lattices, and  $t$  is the neutron time of flight.

### Modeling of Temperature Fields

During EBW the heating of the material is due to the kinetic energy being given to the metal from an electron flow with a power density above  $5.10^6$  W/cm<sup>2</sup>. The accelerated electrons penetrate into depth and, as a result of their interaction with the metal atoms, a melting and evaporation process starts. This forms a vapor-gas channel, called "keyhole". The power of the source  $Q$  [W] is determined by the accelerating voltage  $U$  [kV] and the beam current  $I$  [mA]:  $Q = U \cdot I$ . We assume that the power of the source is distributed between two separate moving sources. The first source is a point source that moves on the surface of the metal and its power is  $Q_1 = 0.1 Q$ . The second one is a linear source and it moves inside the metal with a thickness equal to the depth of the molten pool. Its power is  $Q_2 = 0.9 Q$ . According to the models of moving point and linear sources [9, 3] based on solving the thermal conductivity equation, the temperature at a certain point and a certain moment can be determined using the following equations:

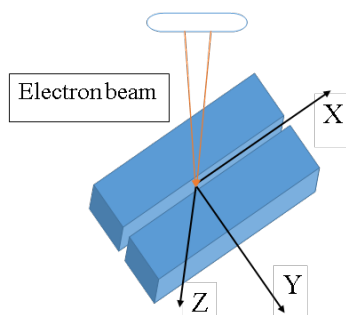
$$T(x, r, \infty) - T_0 = \frac{Q_1}{2\pi\lambda r} e^{-\frac{v(x+r)}{2a}} \quad (5)$$

$$T(x, r, \infty) - T_0 = \frac{Q_2/h}{2\pi\lambda r} e^{-\frac{vx}{2a}} K_0 \left( \frac{vr}{2a} \sqrt{1 + \frac{4ab}{v^2}} \right) \quad (6)$$

where  $r$  is the radius-vector,  $v$  is the welding speed,  $\lambda$  is the heat conductivity,  $h$  is the depth of weld,  $a$  is the thermal conductivity,  $b$  is the coefficient of heat transfer,  $K_0(u)$  is the modified Bessel function of the second kind of order zero.

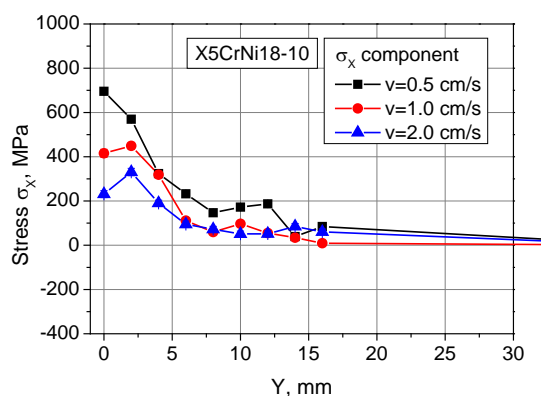
## RESULTS AND DISCUSSIONS

Fig. 2 shows the position of coordinate system axis in relation to the sample for clarity. The specimen is moving along the X-axis. Because of the relative motion we can see that the electron beam moves along the surface of the sample and the displayed coordinate system moves along with the source. The residual stresses are measured along the Y-axis. The temperatures are calculated along the X-axis for different values of the Y-coordinate.



**Fig. 2.** Coordinate system associated with the moving source.

The measured diffraction spectra were processed using the Rietveld method. As a result of these analyses the lattice parameter values dependency *versus* interplanar distance  $d_{hkl}$  were obtained. The residual stresses tensor components in the studied specimens were determined from the obtained lattice parameter values. The dependences of residual stresses from the X-coordinate (across the welding joint) are presented on Figs. 3 - 8.



**Fig. 3.** X-components of residual stress in the studied EBW specimens from X5CrNi18-10 steel during scanning along Y-coordinate across welds for welding speeds  $V=0.5$  cm/s,  $V=1$  cm/s and  $V=2$  cm/s.

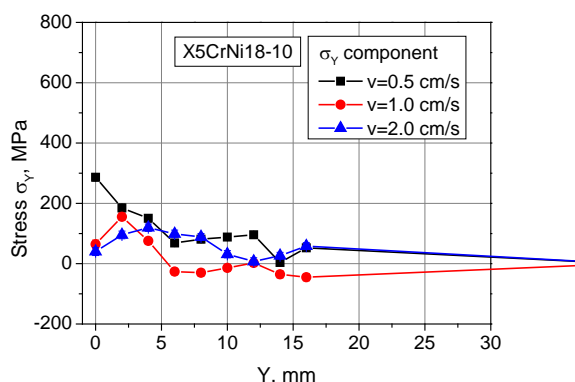


**Fig. 4.** Y-components of residual stress in the studied EBW specimens from X5CrNi18-10 steel during scanning along Y-coordinate across welds for welding speeds  $V=0.5$  cm/s,  $V=1$  cm/s and  $V=2$  cm/s.

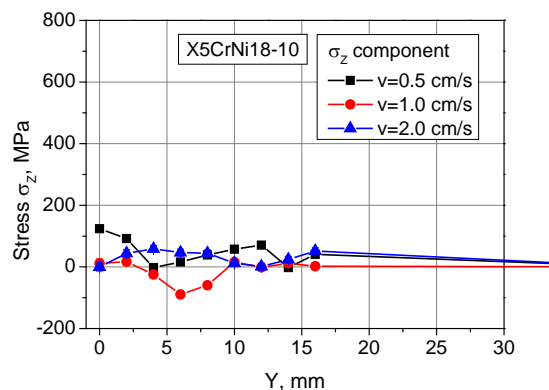


**Fig. 5.** Z-components of residual stress in the studied EBW specimens from X5CrNi18-10 steel during scanning along Y-coordinate across welds for welding speeds  $V=0.5$  cm/s,  $V=1$  cm/s and  $V=2$  cm/s.

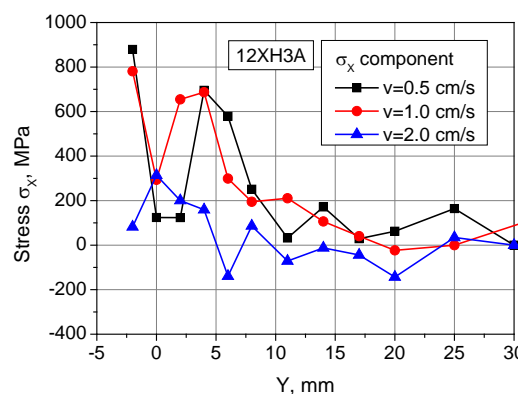


**Fig. 6.** X-components of residual stress in the studied EBW specimens from 12XH3A steel during scanning along Y-coordinate across welds for welding speeds  $V=0.5$  cm/s,  $V=1$  cm/s and  $V=2$  cm/s.

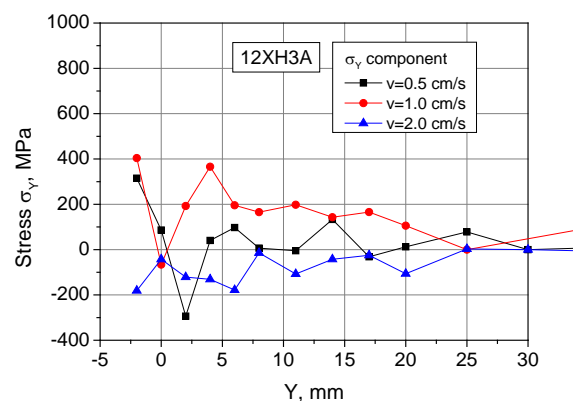


**Fig. 7.** Y-components of residual stress in the studied EBW specimens from 12XH3A steel during scanning along Y-coordinate across welds for welding speeds  $V=0.5$  cm/s,  $V=1$  cm/s and  $V=2$  cm/s.

$V=0.5$  cm/s,  $V=1$  cm/s and  $V=2$  cm/s.

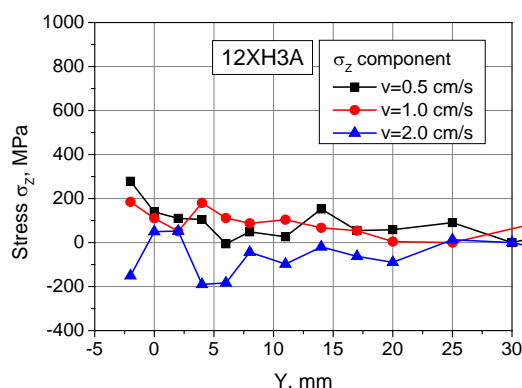


**Fig. 8.** Z-components of residual stress in the studied EBW specimens from 12XH3A steel during scanning along Y-coordinate across welds for welding speeds  $V=0.5$  cm/s,  $V=1$  cm/s and  $V=2$  cm/s.

Residual stresses with alternating signs, i.e. compressive and tensile, are observed. The highest values of the stress are close to the welding seam. They are of the order of 870 MPa for the chrome-nickel steel and of 700 MPa for the constructive one. The residual stresses strongly depend on the electron beam parameters of welding (accelerating voltage, beam current, welding speed). The highest residual stress value is obtained at the lowest welding speed, because the sample receives more energy per unit time at a lower speed.

The calculated temperature cycles for the specimen from X5CrNi18-10 steel is presented on Fig. 9. It shows the change of temperature in the direction of the source movement, respectively in time. At a lower source speed, heating to higher temperature and slower cooling are observed. The closer to the weld seam certain point, the higher is the temperature. Due to imperfections of the model, the temperature at points very close to the source converges to infinity.

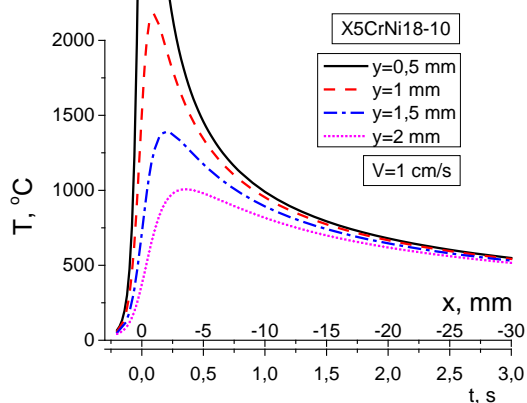


**Fig. 9.** The temperature distribution on X-axis and on time-axis for the studied EBW specimens from X5CrNi18-10 steel along X-coordinate for welding speed  $V=1$  cm/s.

The data from the temperature cycles were used to obtain the dependence between the maximum temperature and Y-coordinate. These dependences for the specimen from X5CrNi18-10 steel for three different welding speeds are shown on Fig. 10.

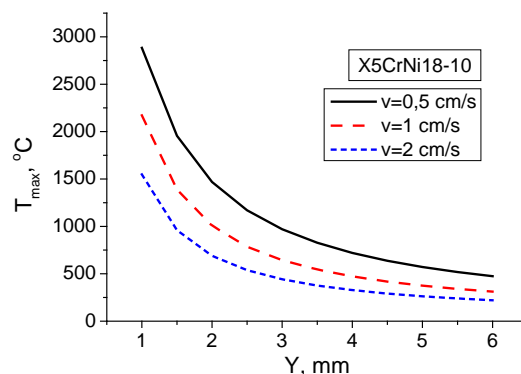


**Fig. 10.** The dependence between the maximum temperature and Y-coordinate for welding speeds  $V=0.5$  cm/s,  $V=1$  cm/s and  $V=2$  cm/s.

The temperature fields for 12XH3A steel are very similar to these of X5CrNi18-10 steel. There are small differences due to different thermophysical parameters.

The calculated data of the temperature field for EBW specimens from X5CrNi18-10 steel presented on Fig. 10 show a very high temperature gradient along the coordinate axis Y. This is the main reason for the experimentally obtained stresses, which are shown on Figs. 3-5. Similar results were obtained for EBW 12XH3A steel.

## CONCLUSION

The residual stress distributions in the flat plate alloyed steel specimens during electron beam welding with different welding speeds were determined using a non-destructive neutron diffraction method. The residual stress level is significantly dependent on welding speed that allows optimization of the welding process by selecting appropriate parameters. The temperature distribution during electron beam welding of alloyed steel shows high gradients which directly affect the residual stresses.

**Acknowledgements:** The authors would like to thank the Bulgarian Nuclear Regulatory Agency for providing financial support and the Bulgarian National Scientific Fund (Contract No. DN 07/26).

## REFERENCES

- 1.D. Radaj, Welding Residual Stresses and Distortion: Calculation and Measurement, second ed., Elsevier, München, 2003.

2. K. Masubuchi, Analysis of welded structure, Pergamon Press, New York, 1980.
3. V. Mihailov, V. Karhin, P. Petrov, Fundamentals of welding (In English), Polytechnic University Publishing, St. Petersburg, 2016.
4. N. S. Rossini, M. Dassitsi, K. Y. Benyounis, A. G. Olabi, *Mater. Design*, **35**, 572 (2012).
5. A.J. Allen, M.T. Hutchings, C.G. Windsor, *Adv. Phys.*, **34**, 445 (1985).
6. L. Pintschovius, in: Measurement of Residual and Applied Stress Using Neutron Diffraction, M.T. Hutchings, A. D. Krawitz (eds.), NATO ASI Series E No 216, Kluwer, Dordrecht, 1992.
7. G.D. Bokuchava, V. L. Aksenov, A. M. Balagurov, E. S. Kuzmin, V. V. Zhuravlev, A. P. Bulkin, V. A. Kudryashev, V. A. Trounov, *Appl. Phys. A- Mater.*, **74** [Suppl. 1], 86 (2002).
8. G. D. Bokuchava, A. M. Balagurov, V. V. Sumin, I. V. Papushkin, *J. Surf. Invest. - X-ray*, **4**, 879 (2010).
9. D. Rosenthal, *Weld. J.*, **20** (5), 220 (1941).